Journal of Materials Research and Technology 34 (2025) 1068–1079

Contents lists available at ScienceDirect

Journal of Materials Research and Technology

journal homepage: www.elsevier.com/locate/jmrt

Enhancing surface integrity of medical Ti–6Al–4V alloy via magnetic field-assisted mass polishing

Rui Gao [a,1], Dawei Luo [a,1], Yee Man Loh [a], Chi Fai Cheung [a,**], Chen Jiang [b], Chunjin Wang [a,*]

[a] State Key Laboratory of Ultra-precision Machining Technology, Department of Industrial and Systems Engineering, The Hong Kong Polytechnic University, Hong Kong, China

[b] College of Mechanical Engineering, University of Shanghai for Science and Technology, Shanghai, 200093, China

ARTICLE INFO

Keywords:
Magnetic field-assisted polishing
Mass finishing
Surface quality
TC4 alloy
Ultra-precision machining

ABSTRACT

The Ti–6Al–4V (TC4) alloy is extensively utilized in the medical industry. However, untreated TC4 alloy exhibits a high degree of roughness, significantly impeding its performance. Enhancing the polishing efficiency of TC4 has thus become a critical focus. This study investigates the feasibility of magnetic field-assisted mass polishing (MAMP) for medical TC4 alloy. A comprehensive series of experimental studies were conducted to evaluate and analyze the surface integrity before and after the polishing process. The empirical results demonstrate the effectiveness of the proposed method for mass polishing TC4 alloy. The polished samples achieved a minimum surface roughness (Sa) of 6.9 nm after 20 min of treatment, with a material removal rate (MRR) of 55.8 nm/min. Post-polishing, the mechanical properties and surface Post-polishing after MAMP, the TC4 samples do not exhibit any significant changes in elemental weight% or phase transformation when compared to the initial samples. Having a smaller surface roughness is advantageous for achieving a higher flexural strength and hardness and improving surface wettability showed slight improvement, with no significant chemical reactions or phase changes observed. This research provides pivotal insights and recommendations for the ultra-precision mass polishing of medical TC4 alloys, potentially offering an optimal solution for polishing various medical components. Furthermore, this study presents straightforward and practical advice that significantly contributes to the advancement of manufacturing processes for medical parts and surface finishing methods.

1. Introduction

Titanium alloy Ti–6Al–4V (TC4) is frequently utilized in a variety of medical applications thanks to its superior biocompatibility and mechanical features [1–3]. These applications include ventricular assist device [4], dental implants [5,6], orthopedic implants [7–10] and so on. Notably, the surface quality of TC4 is crucial for its performance in these applications [11]. When TC4 is used for intestine surgical tools, an increase in surface roughness leads to a decrease in corrosion resistance [12], which can result in a shortened lifespan for the tool [13]. However, TC4 is a challenging material to machine with due to its high strength and hardness [14,15], making it difficult to polish. Therefore, achieving precise and efficient finishing of medical TC4 alloys with accurate form and nanometric surface roughness is an important area of research.

Up to now, previous research has established that mechanical polishing (MP) [16–18], chemical mechanical polishing (CMP) [19–21], plasma electrochemical polishing (PEP) [22–24] and laser polishing (LP) [25–27] are the primary techniques for obtaining precision surfaces of TC4 alloys. Through the optimization of process parameters in belt polishing, Chen et al. [28] focused on enhancing the material removal rate and maintaining superior surface quality of TC4 alloys. DiFelice et al. [29] used a commercial polishing wheel with alumina abrasives and achieved an arithmetic average surface roughness Ra of 300 nm. However, mechanical polishing is inefficient and time-consuming. To decrease surface roughness, Zhang et al. [30] proposed a novel CMP slurry for polishing TC4 alloys, and the polishing slurry included silica, deionized water, malic acid and hydrogen peroxide (H_2O_2). In addition, one study by Ozdemir et al. [31] reported that the roughness Ra of the

* Corresponding author.
** Corresponding author.
E-mail addresses: benny.cheung@polyu.edu.hk (C.F. Cheung), chunjin.wang@polyu.edu.hk (C. Wang).
[1] These authors contributed equally to this work.

https://doi.org/10.1016/j.jmrt.2024.12.081
Received 16 October 2024; Received in revised form 29 November 2024; Accepted 11 December 2024
Available online 12 December 2024

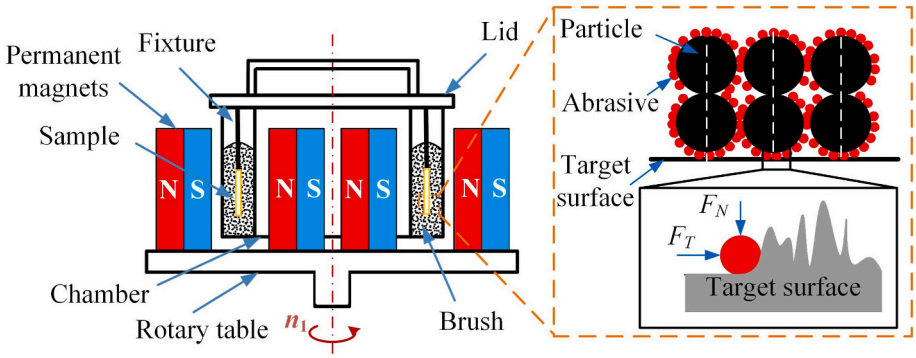

Fig. 1. Schematic diagram of MAMP technique.

Fig. 2. MAMP system. (a) Photograph of experimental setup. (b) Photograph of the chamber with two magnetic brushes. (c) SEM image of magnetic brush. (d) Internal structure photograph of the MAMP. (e) Magnified view of the cap. (f) Polished area and measurement positions.

polished TC4 alloys using CMP was around 128 nm under optimal process conditions. In a study conducted by Bezuidenhout et al. [32], they compared the polishing results of TC4 alloys produced through additive manufacturing, utilizing HF–HNO3 chemical polishing liquid at varying ratios. Compared to the as-built condition, the polished specimens displayed greater fatigue strengths and a reduced number of surface crack initiation sites. Despite being a self-passivating material, TC4 alloy has the capability to quickly establish a protective passive layer. This occurrence can potentially lead to a reduced-efficiency CMP [33]. In terms of electrochemical polishing, Guilherme et al. [34]

Table 1
MAMP experimental parameters.

Items (unit)	Values
Rotation speed (rpm)	600, 900, 1200, 1500, 2000
Weight of magnetic abrasive (g)	60
Polishing time (min)	5, 10, 15, 20
Impinging angle (degree)	15

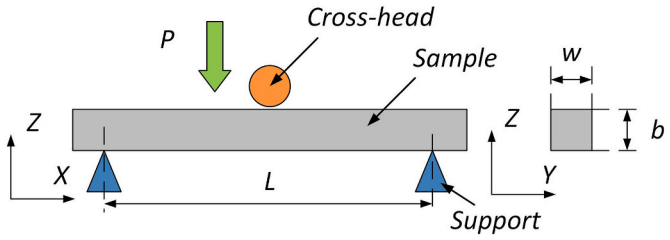

Fig. 3. Schematic diagram of the three-point bending test.

evaluated its feasibility on TC4 alloy polishing and analyzed the influence of surface roughness on corrosion-fatigue strength. In a follow-up study, Wang et al. [35] examined how various electrochemical polishing parameters affected the surface roughness of TC4 alloys. Despite their ability to reduce surface roughness, both chemical and electrochemical polishing techniques remain relatively costly and intricate. Additionally, the electrolyte utilized in this procedure consists of a potent acid or alkali solution that is extremely toxic. This poses a dual threat as it endangers the health of the operators and contributes to pollution in the environment. Ma et al. [36] have shown that fiber laser technology could be used as an environmentally friendly method for polishing the rough surface of additive manufactured TC4 alloys. They were able to achieve a smoothness of 0.375 μm roughness Sa from an initial roughness of 5.226 μm. Similarly, TC4 alloys were polished using a nanosecond pulse laser that emits a wavelength of 1064 nm, resulting in a surface roughness reduction from 5 μm to 2.758 μm [37]. However, the laser polishing process can lead to surface cracking and the formation of metal oxides [38,39], making it challenging to achieve nanoscale roughness.

Compared with the above-mentioned methods, magnetic field-assisted finishing (MAF) has attracted much attention as a promising method for polishing TC4 alloys because of its good flexibility and easy controllability [40–42]. Barman et al. [43,44] reported an MAF tool utilized for producing nano-finished TC4 alloys through the use of magnetorheological (MR) fluids. The obtained surface roughness Ra was 10 nm following 6.3 h of polishing. Fan et al. [45] also developed an MAF tool that contains four permanent magnets. This tool was capable of achieving a surface roughness Ra of 46 nm within 35 min of polishing, starting from an initial value of 1.121 μm. In their study, Parameswari et al. [40] created a machining tool specifically for polishing TC4 alloy flat discs. After dedicating 30 min to polishing, they successfully reduced the initial roughness of 400 nm to a minimum surface roughness Ra of 95 nm, marking a significant improvement. Nevertheless, there remains a pressing issue concerning the efficiency of polishing. These approaches have a drawback: they can only polish samples individually, and it typically takes several tens of minutes to process each sample.

In 2020, our research team successfully developed an innovative

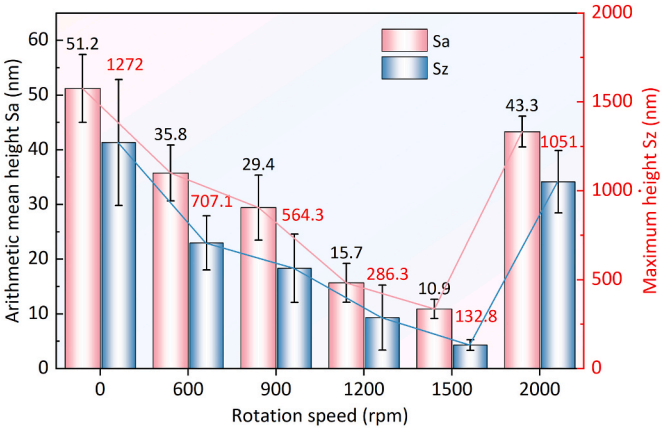

Fig. 5. The relationship between rotation speed and surface roughness with a polishing time of 10 min.

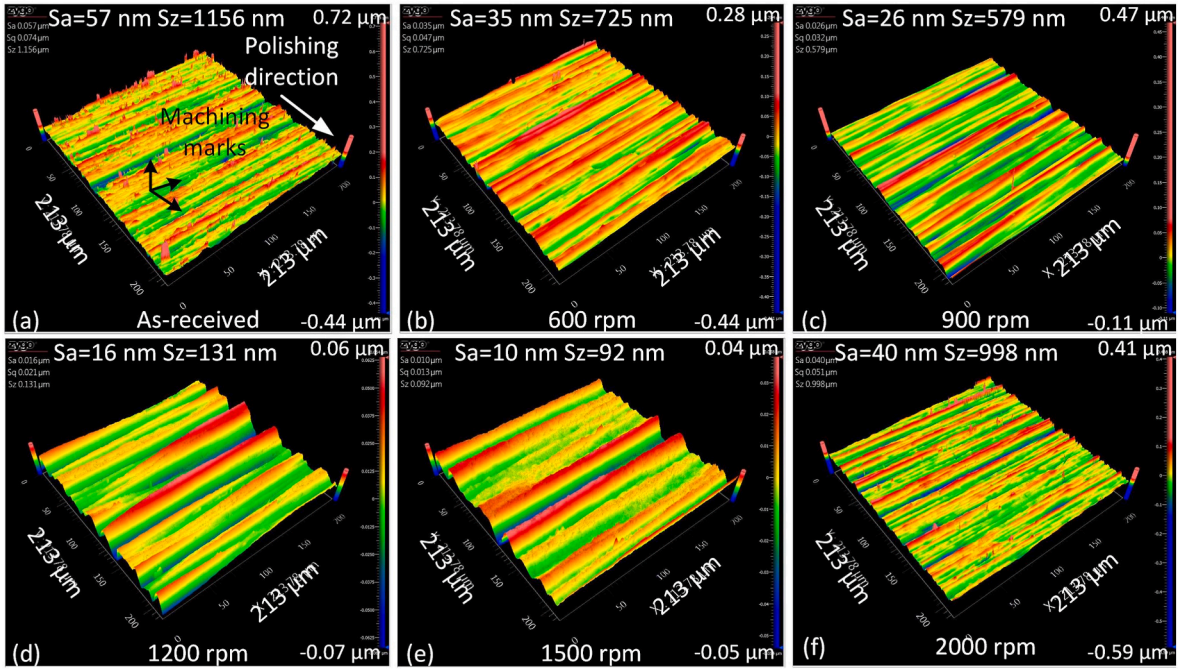

Fig. 4. 3D topography images of the TC4 alloy under various rotation speed. (a) As-received. (b) 600 rpm. (c) 900 rpm. (d) 1200 rpm. (e) 1500 rpm. (f) 2000 rpm.

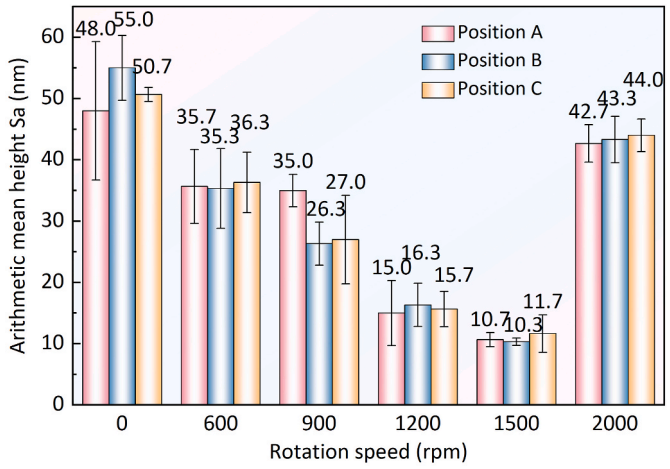

Fig. 6. Surface roughness changing with the rotation speed at three positions with a polishing time of 10 min.

technique called magnetic field-assisted mass polishing (MAMP). This technique has the capability to simultaneously polish a batch of workpieces and achieve nanometric surface roughness [46]. Meanwhile, this approach has been successfully applied in the polishing of 304 stainless steel and dental ceramics [47–49]. Nonetheless, the feasibility on TC4 has not been validated, and our understanding of its material removal mechanism is still far from complete. Furthermore, the potential of MAMP to enhance the polishing efficiency of TC4 alloys has not been demonstrated.

In our current study, we aimed to improve the polishing efficiency of TC4 alloy surfaces by using the MAMP technique. We also sought to achieve nanometric surface roughness and uniform material removal. The rest of this paper is structured as follows. The working principle of the MAMP technique is introduced in Section 2. Section 3 presents the MAMP system and experimental design. In Section 4, the polishing performance of TC4 alloys is analyzed and compared. The proposed polishing process is finally validated by evaluating the polishing performance of an intestine surgical tool made of TC4 alloy.

2. Methodology

Fig. 1 illustrates the working principle of the MAMP technique. In particular, the rotary table is equipped with two pairs of permanent magnets to produce a magnetic field that rotates. This magnetic field shapes the magnetic polishing media into two brushes, which are made up of micrometer magnetic particles and polishing slurry containing nanometer-scale abrasives. Additionally, a group of samples is securely held in place on the lid using the fixtures located inside the chamber. Throughout the polishing process, the magnetic brush continuously impacts the sample, resulting in the removal of micro-nano metric materials in order to achieve the desired polishing outcome.

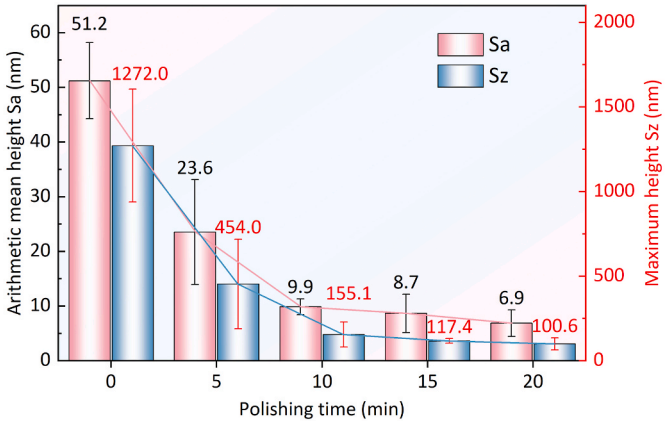

Fig. 8. The relationship between polishing time and surface roughness with a rotation speed of 1500 rpm.

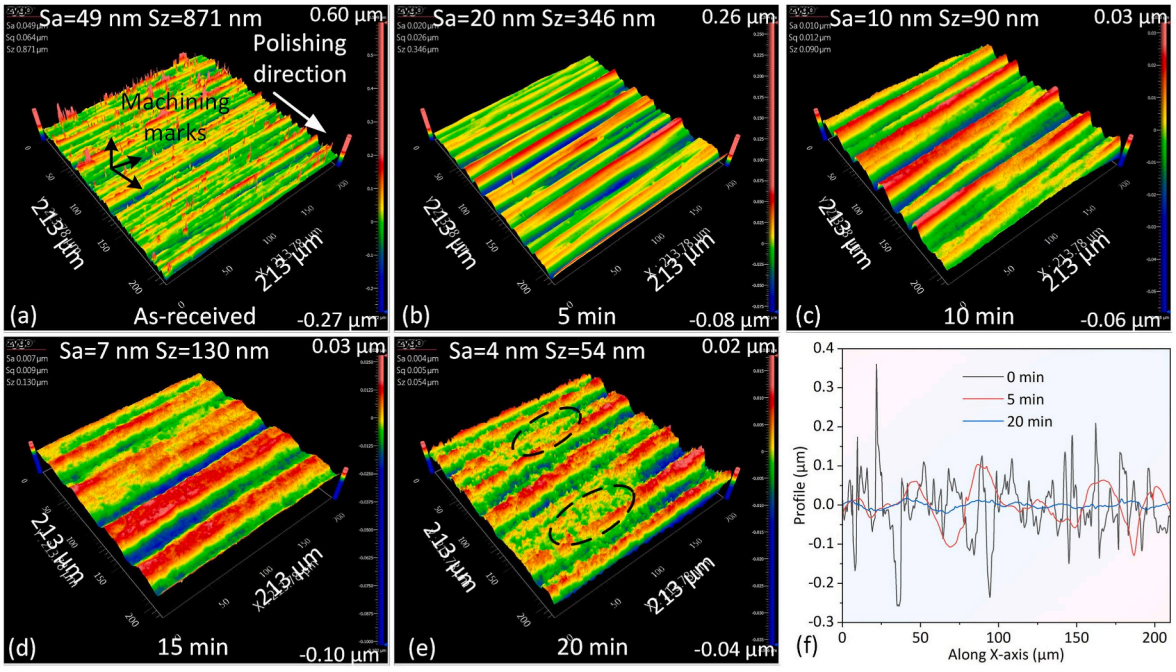

Fig. 7. 3D topography images of TC4 alloys under various polishing times. (a) Initial surface. (b) 5 min. (c) 10 min. (d) 15 min. (e) 20 min. (f) Profile before and after MAMP.

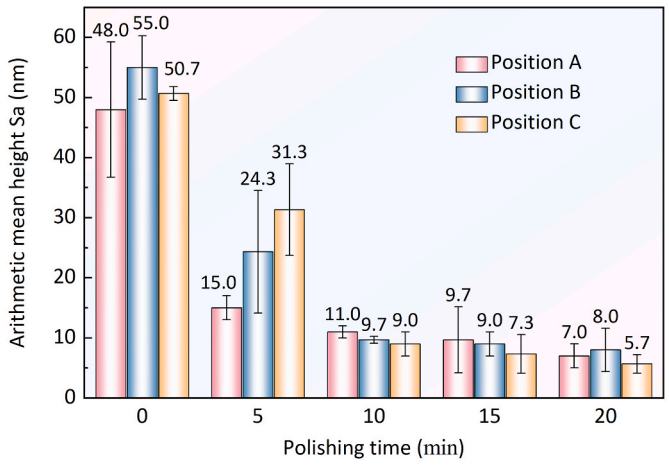

Fig. 9. Surface roughness changing with the polishing time at three positions with a rotation speed of 1500 rpm.

3. Experimental

3.1. Sample preparation

TC4 alloys with a specified chemical composition were used in this study. The TC4 alloy was initially forged and rolled into plates. These plates were then cut into substrates measuring 14 mm × 6 mm × 1 mm using a wire electrical discharge machine. A manual polishing kit was employed to prepare the surface of the samples, resulting in an initial surface roughness Sa of approximately 50 nm.

3.2. Design of experiment

In accordance with the working principle, a corresponding experimental setup was devised, depicted in Fig. 2. The MAMP system comprises a chamber, magnets, a rotary table, and a motor. During the polishing process, the chamber, which is situated over the magnets, stays in a fixed position. The polishing media is then poured into the chamber. The media is comprised of carbonyl iron powder (CIP) averaging about 3 μm in size (75 wt%) and alumina abrasives averaging around 150 nm in size (25 wt%), mixed with the carrying fluid as shown in Fig. 2(c). The carried fluid was water. Two sets of permanent magnets are positioned around the chamber, as illustrated in Fig. 2(d). Samples are held in place by a fixture attached to the cap, as seen in Fig. 2(e). To validate the consistency of the experiments and minimize errors, four samples are polished simultaneously under each condition. The size of the polished area, as depicted in Fig. 2(f), measures 11 mm × 6 mm. As stated in our previous research [47–49], the magnetic field strength of the polishing device used in this study is around 0.4–0.5 T, and additional experimental conditions are listed in Table 1. The samples underwent cleaning for 5 min using an ultrasonic cleaning machine after conducting experiments.

3.3. Surface tests

The surface roughness was measured using a white light interferometer (WLI, NewView, Zygo) to analyze and compare surface topography under different polishing conditions. Surface roughness was evaluated using Sa and Sz, where Sa represents the average arithmetic height of the measured regions and Sz represents the sum of the highest peak height value and the deepest pit depth value within the measured area. The measured region of surface roughness was 213 μm × 213 μm. The calculations for Sa and Sz were carried out using Eqs. (1) and (2)

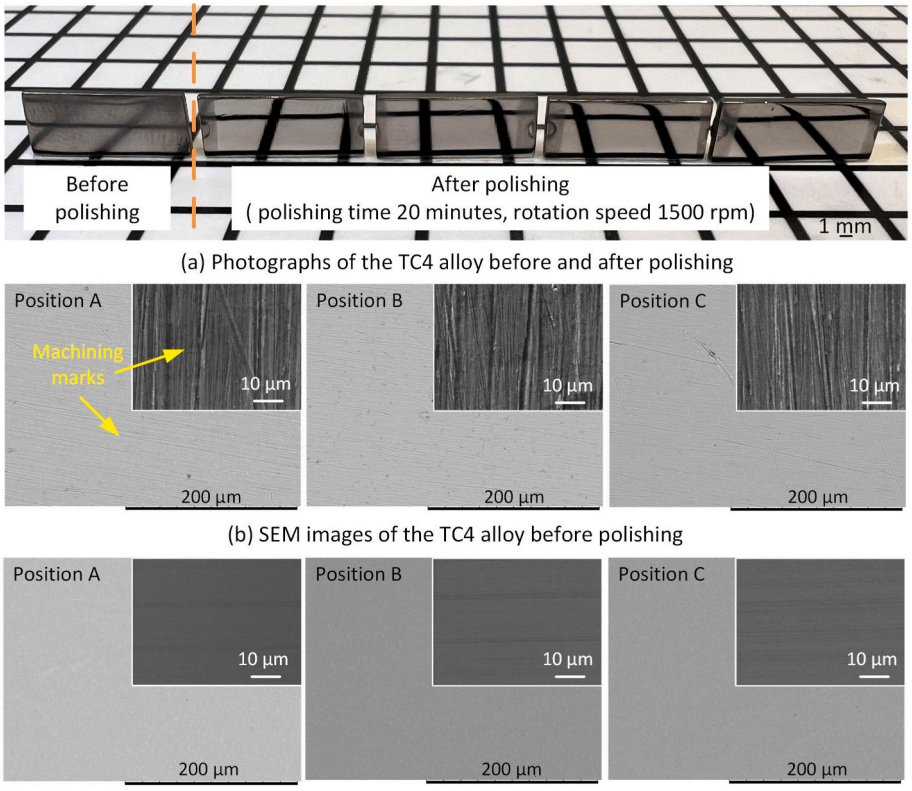

Fig. 10. Polishing performance on TC4 alloy.

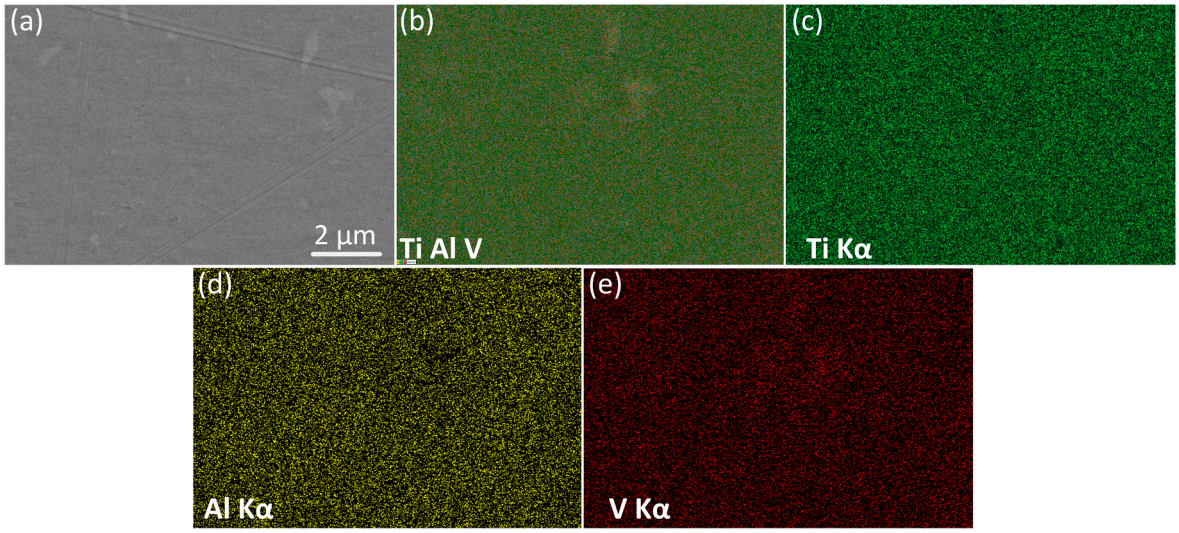

Fig. 11. EDS maps of TC4 alloy after polishing. (a) SE−SEM image. (b) Elemental mapping. (c) Ti. (d) Al. (e) V.

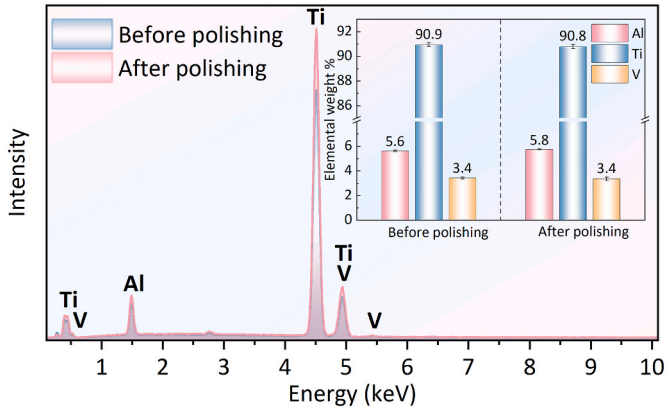

Fig. 12. Location and results of EDS analysis of polished and unpolished TC4 alloy.

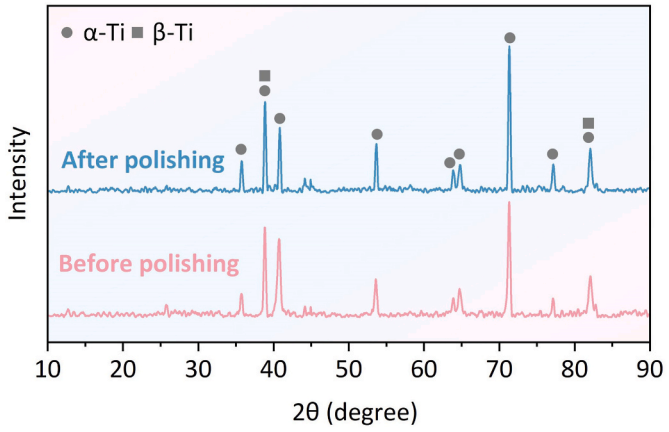

Fig. 13. XRD pattern of polished and unpolished TC4 alloy.

[50,51]. Three measurements of surface roughness were taken at different positions for each polished sample, as depicted in Fig. 2(e). Each position was tested three times to ensure accuracy and repeatability. The average values and standard deviations were determined. Prior to and after polishing, the surface microtopography and elemental composition were inspected using a scanning electron microscope (SEM, TM3000). The sample surface material composition was evaluated with using a Thermo Scientific Apreo 2 SEM equipped with energy-dispersive X-ray spectroscopy (EDS). The phase composition of the TC4 alloys, both polished and unpolished, was analyzed using X-ray diffraction (XRD, Smartlab, Rigaku). The samples were scanned from 10° to 90° with a step size of 0.06°, at a scanning rate of 8°/min.

$$Sa = \frac{1}{A}\iint_A |z(x,y)|dxdy \tag{1}$$

where A represents the region being measured, with x and y indicating the boundaries of the measurement region, $z(x,y)$ represents the height of the machined surface within this region.

$$Sz = Sp + Sv \tag{2}$$

where Sp is the peak and Sv is the valley.

3.4. In-Vito tests

Furthermore, a flexural strength test was conducted on each sample in order to examine the influence of surface finishing. The test followed the ISO 6872 standards for TC4 alloys and employed a universal testing machine. The schematic diagram of the three-point bending test can be seen in Fig. 3. The three-point testing was performed until 6 mm of deflection. To determine the flexural strength, the load applied by a cross-head with a feed rate of 5 mm/min was recorded. To minimize experimental errors, each condition was repeated three times. The flexural strength was calculated using Eq. (3) [47].

$$\sigma = \frac{3PL}{2wb^2} \tag{3}$$

where σ and P denote the flexural strength (MPa) and the load (N) respectively. The distance (mm) between two supports is represented by L and has a fixed value of 12 mm. The thickness (mm) and width (mm) of each sample are denoted by b and w. The Vickers hardness (Wilson Hardness, USA) test was employed to evaluate the micro-hardness of the polished samples. The test followed the ASTM T.1 standards. The indentation experiments were conducted using a load of 300 gf applied for a duration of 10 s. In addition, the dimension of all the samples was about 14 mm in length, 6 mm in width, and 1 mm in thickness for the three-point bending test and Vickers hardness test.

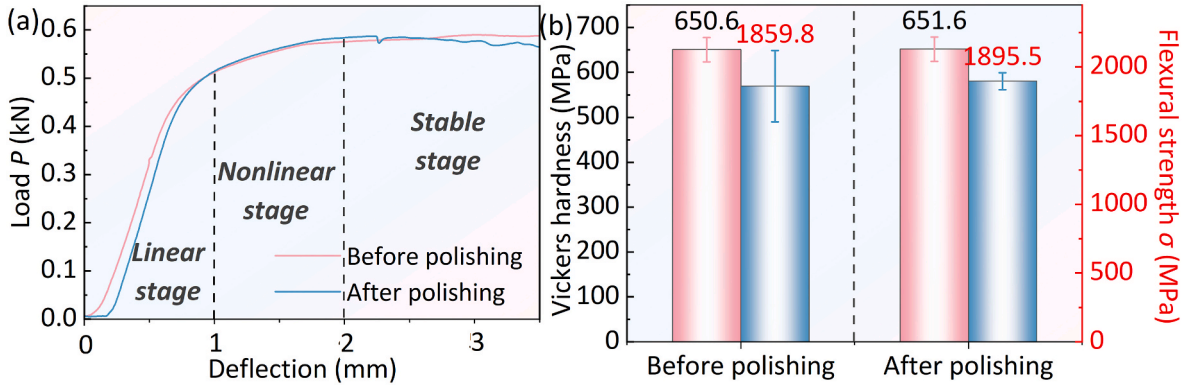

Fig. 14. Three-point bending and hardness test results. (a) Load-deflection curves. (b) Flexural strength and hardness.

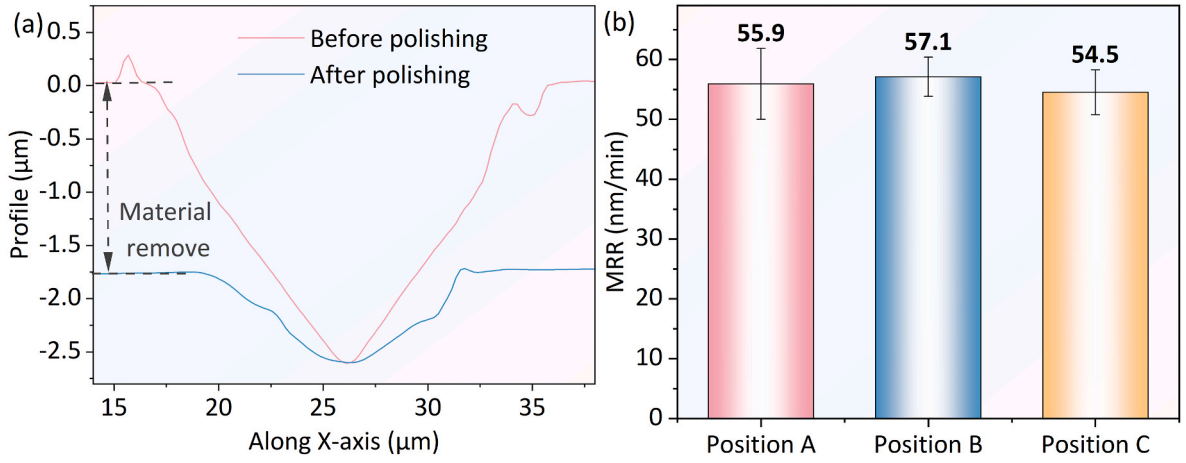

Fig. 15. Material remove test results. (a) Cross-sectional profiles of the Vickers indentation before and after polishing at position A. (b) MRR at three positions.

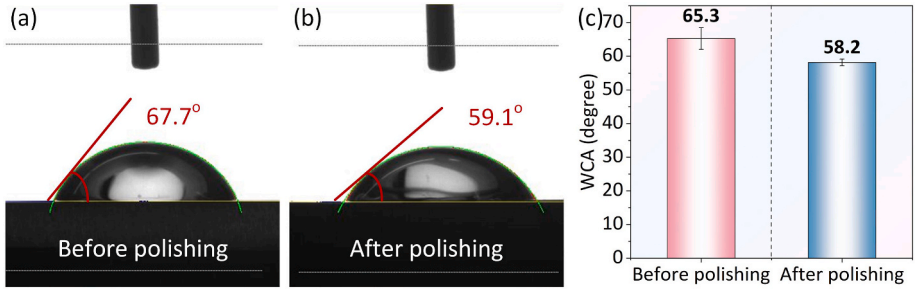

Fig. 16. WCA (a) before and (b) after MAMP at a polishing time of 20 min and a rotation speed of 1500 rpm. (c) Statistics of WCA.

3.5. Material removal rate

To determine the MRR during the polishing of TC4 alloy, a methodology involving Vickers indentation was employed. To investigate the polishing uniformity, three points were indented with a load of 100g at each position, as illustrated in Fig. 2(f). Additionally, the profile of the Vickers indentation before and after polishing the TC4 alloy was measured using a white light interferometer (WLI, NewView, Zygo). Based on the experimental results, the optimal parameters were identified. The polishing time and impinging angle were set to 30 min and 15°, respectively.

3.6. Surface wettability test

The water contact angle (WCA) measurement was conducted to evaluate the wettability of the sample surfaces. An optical video-based contact angle meter (Sindatek, 100SB) was employed to measure the static contact angles at room temperature. A droplet of deionized water (approximately 5 μL) was carefully placed on the surface using a precision syringe. The contact angle was determined by analyzing the shape of the droplet with image analysis software. Each measurement was repeated three times at different locations on the sample to ensure reproducibility and accuracy. The average contact angle values were then calculated.

4. Results and discussions

4.1. Effect of rotation speed

Fig. 4 presents the 3D topography images of TC4 alloys at various

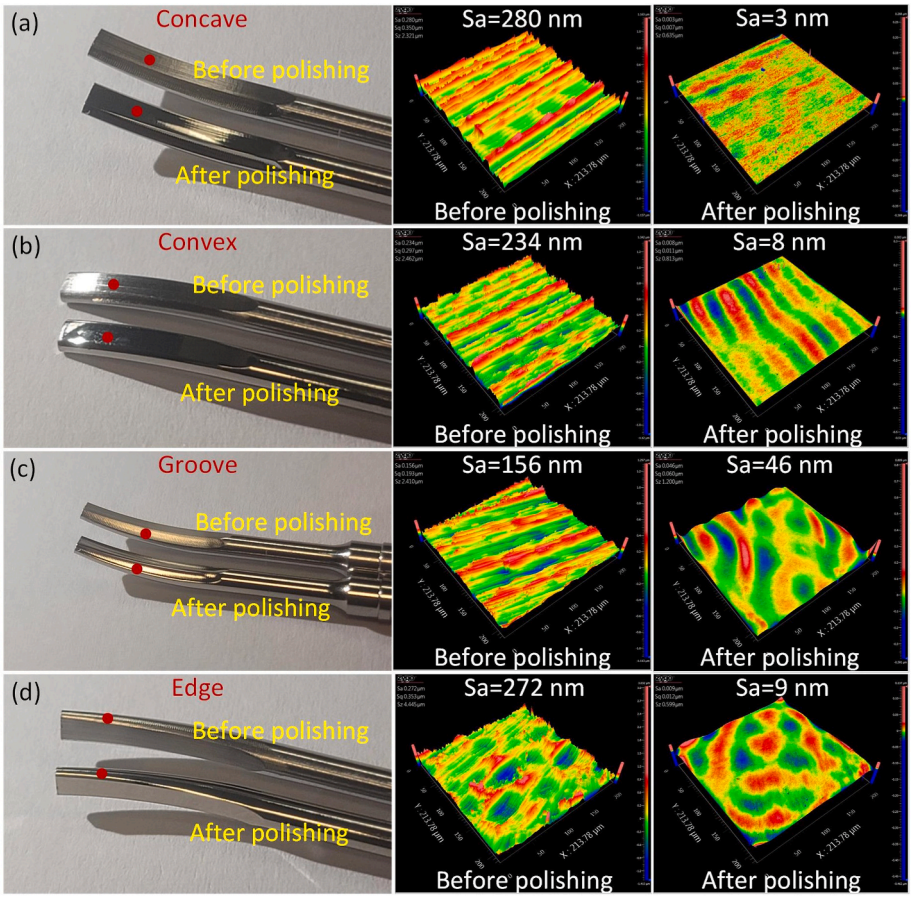

Fig. 17. Polishing performance on TC4 intestine surgical tool at a polishing time of 10 min and a rotation speed of 1500 rpm. (a) Concave. (b) Convex. (c) Groove. (d) Edge. The corresponding positions have been pointed out by the red dot.

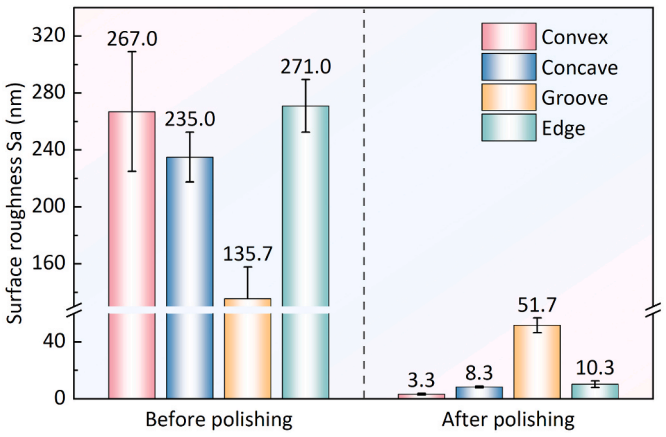

Fig. 18. Summary of average surface roughness on each surface of the intestine surgical tool before polishing and after polishing (polishing time 10 min, rotation speed 1500 rpm).

rotation speeds, with a constant polishing time of 10 min. The specific test position selected is position B. As depicted in Fig. 4(a), the surface of the as-received sample exhibits uneven machining marks due to rough lapping, resulting in significant surface height waviness. To mitigate these tool marks and surface height waviness, the polishing direction was oriented perpendicular to the machining marks. The graph demonstrates a notable reduction in surface roughness as the rotation speed increases, up to 1500 rpm. Under these conditions, the values for Sa and Sz are 10 nm and 92 nm, respectively, indicating a substantial decrease in surface waviness. However, as shown in Fig. 4(f), the surface roughness increases when the rotation speed is further elevated to 2000 rpm.

Table 2
General comparison between different polishing methods.

Method	Source	Number of samples	Surface roughness	Polishing efficiency	Polishing cost
MP	Ref [16]	1	Ra = 400 nm	Low	Medium
	Ref [51]	1	Ra = 200 nm	Low	Medium
LP	Ref [22]	1	Ra = 77 nm	Medium	High
	Ref [52]	1	Sa = 1127 nm	Medium	High
CMP	Ref [26]	1	Ra = 0.68 nm	Low	Medium
	Ref [53]	1	Ra = 1.90 nm	Low	Medium
MAMP	Our work	≤4	Sa = 6.9 nm	High	Low

Fig. 5 provides the effect of rotation speed on surface roughness, specifically Sa and Sz, at a polishing time of 10 min. The surface roughness of TC4 alloys gradually decreased as the rotation speed increased, until it reached 1500 rpm. Starting from 51.2 nm before polishing, the average value of Sa steadily decreased to 35.8 nm, 29.4 nm, 15.7 nm, and finally 10.9 nm at a rotation speed of 1500 rpm. Similarly, Sz showed a gradual decrease from 600 rpm to 1500 rpm. However, when the rotation speed reached 2000 rpm, there was a sharp

increase in the average values of Sa and Sz, reaching 43.3 nm and 1051.2 nm, respectively. This increase in surface roughness can be attributed to the centrifugal force, which becomes stronger with an increase in rotation speed, leading to an increase in the frictional force exerted on each abrasive [52]. Despite the magnetic force, the frictional force cannot be overcome, resulting in irregular jumbling of the magnetic abrasives. This irregular jumbling causes aggressive impact on the workpiece surface, thus affecting the surface integrity. Wang et al. [49] also reported a similar phenomenon.

Fig. 6 shows the summary statistics for surface roughness Sa changing with the rotation speed in three different positions. It can be obviously seen that the average value of Sa declines sharply with increase of the rotation speed for all the positions. What stands out in this figure is that average values of Sa in position A, B and C at rotation speed of 1500 rpm are 10.7 nm, 10.3 nm and 11.7 nm, respectively. It indicates that the whole surface exhibits quite uniform polishing performance.

4.2. Effect of polishing time

Fig. 7 illustrates the 3D topography images of TC4 alloys at different polishing times, maintaining a constant rotation speed of 1500 rpm. All images correspond to test position B. Initially, the surface of the TC4 alloy exhibits numerous uneven machining marks, as shown in Fig. 7(a). However, with increasing polishing time, the height of these machining marks significantly decreases. After 5, 10, and 15 min of polishing, the surface roughness is reduced to 20 nm, 10 nm, and 7 nm, respectively. Notably, after 20 min of polishing, some areas, highlighted by a black circle in Fig. 7(e), show complete removal of machining marks, resulting in a smoother workpiece surface. The measurements of Sa and Sz after polishing are 4 nm and 54 nm, respectively, indicating that machining marks can be effectively eliminated using MAMP.

The relationship between surface roughness and polishing time at the rotation speed of 1500 rpm can be seen in Fig. 8. Similar to the experiment results in Section 4.1, the average values of surface roughness drop significantly as the polishing time increases. Firstly, starting from 51.2 nm, the average value of Sa plunges to 9.9 nm after 10 min of polishing and is followed by another moderate decrease to 6.9 after 20 min of polishing. Meanwhile, the same trend can also be observed in Sz. After 20 min of polishing, the average value of Sz is 100.6 nm.

As shown in Fig. 9, the summary statistics for surface roughness Sa are presented in relation to the polishing time at three different positions. At position A, the average Sa value significantly reduces from an initial 48.0 nm–15.0 nm after 5 min of polishing. Conversely, there is a minor decrease in the average Sa value at positions B and C. After polishing for 20 min, the average Sa values at these three positions are 7.0 nm, 8.0 nm, and 5.7 nm, respectively.

Fig. 10(a) provides the photographs of the TC4 alloy samples before and after a 20 min-polishing process at a rotation speed of 1500 rpm. The desired mirror effect is successfully achieved for all the samples. Furthermore, SEM images of TC4 alloy at three varied positions, both before and after a 20-min MAMP polishing, are illustrated in Fig. 10 (b–c). Prior to polishing, clear machining marks resulting from shaping and manual lapping are evident at all three positions for the as-received samples. However, after 20 min of MAMP, Fig. 10(c) clearly illustrates a smooth surface with minimal micro-defects. This demonstrates the precise batch polishing capability of the proposed technique utilized in this study for TC4 alloys.

4.3. EDS and XRD analysis

In order to examine whether there were any changes in material and phase transformation before and after polishing, EDS and XRD tests were conducted. For the polished sample in this section, the polishing time and rotation speed were 20 min and 1500 rpm, respectively. The TC4 material used in this study primarily consists of Al, Ti, and V, and the surface elemental composition remains essentially unchanged after polishing, as shown in Figs. 11 and 12. This discovery was also reported by Ke et al. [53]. Additionally, there is a slight increase of about 1% in the weight% of Al after polishing, while the weight% of V decreases by approximately 1%. As for the Ti element, there is a moderate fluctuation observed in its weight%.

The XRD pattern (seen in Fig. 13) clearly illustrates the phase constitution of the (α+β) dual phases in the TC4 alloy, with α-Ti being the main phase. Furthermore, the XRD patterns of the polished samples exhibit a similar pattern of main and minor peaks. However, there is a slight increase in peak strength in comparison to the unpolished samples. This could potentially be due to alterations in surface roughness, which may be attributed to changes in surface roughness. Overall, these findings indicate that there are no significant alterations in the material and phase composition following MABP polishing. This may be due to the absence of mechanical load-induced grain refinement, high temperatures, or chemical reactions during the process.

4.4. Flexural strength and hardness tests

In Fig. 14(a), the load-deflection curves of the unpolished and polished samples are present. The polishing time and rotation speed were 20 min and 1500 rpm, respectively. These curves can be categorized into three stages: linear stage, nonlinear stage, and stable stage, with minor differences observed in these stages. The average flexural strength and Vickers hardness value for both polished and unpolished samples is illustrated in Fig. 14(b). It is worth mentioning that the flexural strength (1895.47 MPa) and hardness (651.6 MPa) of the polished samples are slightly larger than those (1859.80 MPa and 650.6 MPa) of the unpolished samples. This can be attributed to the visible scratches on the surface (Fig. 10), which have the potential to generate unexpected cracks [54].

4.5. MRR tests

To elucidate the MRR in the context of MAMP for TC4 alloy, the material removal test results are presented in Fig. 15. The rotation speed is set at 1500 rpm. Fig. 15(a) illustrates the cross-sectional profiles of the Vickers indentation before and after polishing at position A. It can be observed that MAMP achieves a maximum material removal depth of approximately 1.8 μm. Furthermore, the average MRR values at the three positions are 55.9 nm/min, 57.1 nm/min, and 54.5 nm/min, respectively as shown in Fig. 15(b). This indicates that the entire surface exhibits a highly uniform polishing performance.

4.6. Wettability test

Surface wettability testing of medical TC4 is crucial for evaluating its biocompatibility [55]. A surface with optimal wettability can promote better cell attachment and proliferation, thereby enhancing its performance in medical applications such as implants and prosthetics [56]. Improved wettability can lead to reduced inflammation and faster healing, ultimately contributing to the overall success of medical devices made from TC4. Fig. 16(a–b) illustrate the optical images of water contact angle (WCA) on medical TC4 before and after polishing. The polished sample is prepared using optimal parameters: a rotational speed of 1500 rpm and a polishing time of 20 min. It can be observed that the WCA decreases after MAMP treatment, with the average values of WCA before and after polishing being 65.3°and 58.2°as shown in Fig. 16(c), respectively. This indicates that the hydrophilicity of the MAMP-processed TC4 improves.

4.7. Verification test on TC4 intestine surgical tool

To test the feasibility of MAMP, an experiment was conducted on the intestine surgical tool made from TC4 alloy. It was initially forged to achieve the desired shape. The forged blank was then cut and milled into

the form of the surgical tool. The machined tool underwent heat treatment processes to enhance its mechanical properties and toughness. The rotation speed used was 1500 rpm, and all other experimental parameters remained the same as stated in Table 1. To evaluate the polishing performance, four specific surfaces of the intestine surgical tool were chosen: concave, convex, groove, and edge. The ZYGO Nexview white light interferometer was used to measure the surface roughness Sa. An average surface roughness was determined by measuring three separate positions on each surface. The results of the experiment, shown in Fig. 17, demonstrate the polishing performance of MAMP on the TC4 intestine surgical tool. It can be observed that the polished workpiece reflects a much clearer image compared to the unpolished one on all four surfaces, leading to an overall improvement in surface roughness.

The average surface roughness of each surface was summarized in Fig. 18, both before polishing and after 10 min of polishing. Examining the results of the experiment, it was observed that the surface roughness of convex, concave, and edge surfaces experienced a significant decrease. Among them, convex surface exhibited the lowest surface roughness value of 3.3 nm. However, the groove surface was not fully polished, with the surface roughness reducing from Sa 136.0 nm to Sa 51.7 nm.

4.8. Discussion

Currently, a significant proportion of biomedical devices are fabricated from the TC4 alloy, with their operational performance being substantially influenced by surface quality [8,57]. Consequently, there is an urgent need to identify an efficient polishing method for the TC4 alloy to enhance surface quality. In this study, we have demonstrated that the proposed MAMP method can facilitate precision batch polishing of medical TC4 alloy, with the potential to achieve a minimum average surface roughness of Sa 6.9 nm at a polishing time of 20 min and a rotation speed of 1500 rpm. Various existing polishing methods have been used on the TC4 alloy. In this study, we compare the results of our method with other techniques such as MP [16,58], PEP, LP [59,60], and CMP [30,61], as detailed in Table 2. This comparison evaluates the performance of these methods on TC4 based on surface roughness, polishing efficiency, and cost. The CMP method achieves the lowest roughness value, followed by our proposed method and laser polishing. However, CMP has suboptimal efficiency and a relatively high cost [62,63]. Additionally, mechanical polishing does not meet the required surface roughness standard. In contrast, MAMP is able to successfully batch polish the TC4 alloy, achieving nanometric surface roughness. As a result, MAMP is a potentially appealing polishing method that can reduce polishing time and achieve lower surface roughness.

Although there are promising results, there are still certain limitations to this method. One main concern is the uneven surface roughness on the polished TC4 intestine surgical tool, as shown in Fig. 17(c). This discrepancy needs to be improved in future studies. During the polishing process, adjusting the motion of the magnetic brush is a potential solution. Additionally, it is important to gain a more thorough understanding of this new process, as it could offer more valuable insights for practical polishing applications.

5. Conclusion

This research examines the viability of employing magnetic field-assisted mass polishing (MAMP) for medical-grade TC4 alloy. Specifically, our current study aims to enhance the polishing efficiency of TC4 alloy surfaces through the application of the MAMP technique. The key findings from the investigation are as follows.

(1) MAMP emerges as an effective strategy for polishing medical TC4 alloy, achieving nanometric surface roughness within a minimal time frame. Moreover, MAMP enables the simultaneous polishing of multiple TC4 components, ensuring excellent polishing uniformity.
(2) The surface roughness Sa of the polished samples exhibits a progressive reduction as the polishing time extends. Moreover, there is an initial decrease in roughness when the rotation speed increases, but it eventually increases again, suggesting that the optimal rotation speed is 1500 rpm.
(3) A polishing duration and rotation speed of 20 min and 1500 rpm, respectively, yield the minimum average surface roughness, reaching Sa 6.9 nm. The MRR of the MAMP in TC4 polishing is around 55.8 nm/min.
(4) Post-polishing after MAMP, the TC4 samples do not exhibit any significant changes in elemental weight% or phase transformation when compared to the initial samples. Having a smaller surface roughness is advantageous for achieving a higher flexural strength and hardness and improving surface wettability.
(5) The MAMP-processed TC4 intestine surgical tool demonstrates an average surface roughness (Sa) of 3.3 nm on convex regions, 8.3 nm on concave regions, 10.3 nm on edges, and 51.7 nm on grooves following a 10-min MAMP treatment.

These results highlight the promise of MAMP as a technique that can improve the surface quality of medical TC4 alloys, thereby contributing to the advancement of medical component manufacturing processes.

Declaration of competing interest

The authors declare that they have no known competing financial interests or personal relationships that could have appeared to influence the work reported in this paper.

Acknowledgments

The work described in this paper was mainly supported by a Shenzhen-Hong Kong-Macau Technology Research Programme from Shenzhen Science and Technology Innovation Committee (Project No: SGDX20220530110804030), a grant from the Research Grants Council of the Government of the Hong Kong Special Administrative Region, China (Project No. 15203620), State Key Laboratory of Mechanical System and Vibration (Project code: MSV202315), the funding support from the Hong Kong Polytechnic University (Project codes: 1-W308 and 1-BECE) and the research studentships (Project codes: RH3Y).

References

[1] Zhao GX, Zhang J, Zhang SZ, Wang G, Han JC, Zhang CJ. Interfacial microstructure and mechanical properties of TiAl alloy/TC4 titanium alloy joints diffusion bonded with CoCuFeNiTiV0.6 high entropy alloy interlayer. J Alloy Compd 2023;935:167987. https://doi.org/10.1016/j.jallcom.2022.167987.
[2] Guo YQ, Guan J, Peng H, Shu X, Chen L, Guo HB. Tightly adhered silk fibroin coatings on Ti6Al4V biometals for improved wettability and compatible mechanical properties. Mater Design 2019;175:107825. https://doi.org/10.1016/j.matdes.2019.107825.
[3] Chen Y, Yang WX, Zhu S, Shi YS. Microstructural, mechanical and in vitro biological properties of Ti6Al4V-5Cu alloy fabricated by selective laser melting. Mater Charact 2023;200:112858. https://doi.org/10.1016/j.matchar.2023.112858.
[4] DeVore AD, Patel PA, Patel CB. Medical management of patients with a left ventricular assist device for the non-left ventricular assist device specialist. Jacc-Heart Fail 2017;5:621–31. https://doi.org/10.1016/j.jchf.2017.06.012.
[5] Qin W, Ma J, Liang Q, Li JD, Tang B. Tribological, cytotoxicity and antibacterial properties of graphene oxide/carbon fibers/polyetheretherketone composite coatings on Ti-6Al-4V alloy as orthopedic/dental implants. J Mech Behav Biomed 2021;122:104659. https://doi.org/10.1016/j.jmbbm.2021.104659.
[6] Huang L, Luo Z, Hu Y, Shen XK, Li MH, Li LQ, Zhang Y, Yang WH, Liu P, Cai KY. Enhancement of local bone remodeling in osteoporotic rabbits by biomimic multilayered structures on Ti6Al4V implants. J Biomed Mater Res 2016;104:1437–51. https://doi.org/10.1002/jbm.a.35667.
[7] Deng HY, Xu KX, Liu SG, Zhang CF, Zhu XW, Zhou HR, Xia CQ, Shi CB. Impact of engineering surface treatment on surface properties of biomedical TC4 alloys under a simulated human environment. Coatings 2022;12:157. https://doi.org/10.3390/coatings12020157.

[8] Zou X, Jiang MY, Chen K, Chen BX, Reddy KM, Zhang SY, Kondoh K, Wang M, Hua XM, Zhang LT, Shan AD. Mechanism of defect formation during friction spot joining of 3D-printed TC4 alloy and ultra-high molecular weight polyethylene. Mater Design 2020;195:108989. https://doi.org/10.1016/j.matdes.2020.108989.
[9] Wang CC, Hu HX, Li ZP, Shen YF, Xu Y, Zhang GQ, Zeng XQ, Deng J, Zhao SC, Ren TH, Zhang YD. Enhanced osseointegration of titanium alloy implants with laser microgrooved surfaces and graphene oxide coating. Acs Appl Mater Inter 2019;11:39470–83. https://doi.org/10.1021/acsami.9b12733.
[10] Eliaz N. Corrosion of metallic biomaterials: a review. Materials 2019;12:407. https://doi.org/10.3390/ma12030407.
[11] Gao YK. Surface modification of TC4 titanium alloy by high current pulsed electron beam (HCPEB) with different pulsed energy densities. J Alloy Compd 2013;572: 180–5. https://doi.org/10.1016/j.jallcom.2013.04.002.
[12] Ezugwu EO, Wang ZM. Titanium alloys and their machinability - a review. J Mater Process Tech 1997;68:262–74. https://doi.org/10.1016/S0924-0136(96)00030-1.
[13] Xin GQ, Wu CY, Liu WN, Rong YM, Huang Y. Anti-corrosion superhydrophobic surfaces of Al alloy based on micro-protrusion array structure fabricated by laser direct writing. J Alloy Compd 2021;881:160649. https://doi.org/10.1016/j.jallcom.2021.160649.
[14] Xin GQ, Wu CY, Cao HY, Liu WN, Li B, Huang Y, Rong YM, Zhang GJ. Superhydrophobic TC4 alloy surface fabricated by laser micro-scanning to reduce adhesion and drag resistance. Surf Coat Tech 2020;391:125707. https://doi.org/10.1016/j.surfcoat.2020.125707.
[15] Sartori S, Ghiotti A, Bruschi S. Solid lubricant-assisted minimum quantity lubrication and cooling strategies to improve Ti6Al4V machinability in finishing turning. Tribol Int 2018;118:287–94. https://doi.org/10.1016/j.triboint.2017.10.010.
[16] Axinte DA, Kwong J, Kong MC. Workpiece surface integrity of Ti-6-4 heat-resistant alloy when employing different polishing methods. J Mater Process Tech 2009; 209:1843–52. https://doi.org/10.1016/j.jmatprotec.2008.04.046.
[17] Huai WB, Shi YY, Tang H, Lin XJ. Sensitivity of surface roughness to flexible polishing parameters of abrasive cloth wheel and their optimal intervals. J Mech Sci Technol 2017;31:865–73. https://doi.org/10.1007/s12206-017-0140-2.
[18] Chen Z, Zhao P, Yan R, Tian G, Yang M, Shi Y. Quantitative finite element analysis of microscopic surface formation for TC4 aeroengine blade polishing using single-grain method. Int J Adv Manuf Tech 2024;132:2941–55. https://doi.org/10.1007/s00170-024-13515-w.
[19] Balyakin A, Zhuchenko E, Nosova E. Study of heat treatment impact on the surface defects appearance on samples obtained by selective laser melting of Ti-6Al-4V during chemical polishing. Mater Today Proc 2019;19:2307–11. https://doi.org/10.1016/j.matpr.2019.07.676.
[20] Li PF, Wang YH, Li LL, Gong YD, Zhou JZ, Lu JZ. Ablation oxidation and surface quality during laser polishing of TA15 aviation titanium alloy. J Mater Res Technol 2023;23:6101–14. https://doi.org/10.1016/j.jmrt.2023.02.209.
[21] Hou X, Li JY, Li YZ, Tian Y. Intermolecular and surface forces in atomic-scale manufacturing. Int J Extreme Manuf 2022;4:022002. https://doi.org/10.1088/2631-7990/ac5e13.
[22] Zou YC, Wang SQ, Chen GL, Wang YM, Zhang KW, Zhang CR, Wei DQ, Ouyang JH, Jia DC, Zhou Y. Optimization and mechanism of precise finishing of TC4 alloy by plasma electrolytic polishing. Surf Coat Tech 2023;467:129696. https://doi.org/10.1016/j.surfcoat.2023.129696.
[23] Yi R, Zhang Y, Zhang XQ, Fang FZ, Deng H. A generic approach of polishing metals via isotropic electrochemical etching. Int J Mach Tool Manu 2020;150:103517. https://doi.org/10.1016/j.ijmachtools.2020.103517.
[24] Wang J, Sun HW, Yang DL, Ji GQ, Duan HD, Xiang YX. Local surface smoothness on TC4 alloy during microbubbles flow electrolytic plasma polishing: prototype rig, phenomena, and mechanism. Int J Adv Manuf Tech 2024;134:1879–92. https://doi.org/10.1007/s00170-024-14240-0.
[25] Huang XD, Wang T, Hu SW, Yao T, Miao RP, Kang QC, Zhang YZ. Parameter optimization of laser polishing based on orthogonal experiment and response surface method. Laser Optoelectron P 2022;59:1114004. https://doi.org/10.3788/Lop202259.1114004.
[26] Walker D, Ahuir-Torres JI, Akar Y, Bingham PA, Chen X, Darowski M, Fähnle O, Gambron P, Jackson FF, Li H, Mason L, Mishra R, Shahjalal A, Yu G. Bridging the divide between iterative optical polishing and automation. Nanomanufacturing and Metrology 2023;6:26. https://doi.org/10.1007/s41871-023-00197-3.
[27] Shen S, Chen X, Chen J, Zhang W. Influence of laser power and rotational speed on the surface characteristics of rotational line spot nanosecond laser ablation of TC4 titanium alloy. Materials 2024;17:4271. https://doi.org/10.3390/ma17174271.
[28] Chen Z, Shi YY, Lin XJ. Evaluation and improvement of material removal rate with good surface quality in TC4 blisk blade polishing process. J Adv Mech Des Syst 2018;12:18–193. https://doi.org/10.1299/jamdsm.2018jamdsm0083.
[29] DiFelice RA, Dillard JG, Yang D. Chemical and nanomechanical properties of plasma-polymerized acetylene on titanium and silicon. Int J Adhes Adhes 2005;25: 342–51. https://doi.org/10.1016/j.ijadhadh.2004.11.004.
[30] Zhang ZY, Shi ZF, Du YF, Yu ZJ, Guo LC, Guo DM. A novel approach of chemical mechanical polishing for a titanium alloy using an environment-friendly slurry. Appl Surf Sci 2018;427:409–15. https://doi.org/10.1016/j.apsusc.2017.08.064.
[31] Ozdemir Z, Ozdemir A, Basim GB. Application of chemical mechanical polishing process on titanium based implants. Mat Sci Eng C-Mater 2016;68:383–96. https://doi.org/10.1016/j.msec.2016.06.002.
[32] Bezuidenhout M, Ter Haar G, Becker T, Rudolph S, Damm O, Sacks N. The effect of HF-HNO chemical polishing on the surface roughness and fatigue life of laser powder bed fusion produced Ti6Al4V. Mater Today Commun 2020;25:101396. https://doi.org/10.1016/j.mtcomm.2020.101396.
[33] Deng CB, Jiang L, Qian LM. High-efficiency chemical mechanical polishing of Ti-6Al-4V alloy via the synergistic action of H2O2 and K+under alkaline conditions. Ecs J Solid State Sc 2022;11:024005. https://doi.org/10.1149/2162-8777/ac495e.
[34] Guilherme AS, Henriques GEP, Zavanelli RA, Mesquita MF. Surface roughness and fatigue performance of commercially pure titanium and Ti-6Al4V alloy after different polishing protocols. J Prosthet Dent 2005;93:378–85. https://doi.org/10.1016/j.prosdent.2005.01.010.
[35] Wang SF, Wang Y, Wen JC, Suo HL, Liu ZZ, Suo WH, Zhao CC. Study on electrochemical polishing of TC4 alloy. Mater Res Express 2021;8:106520. https://doi.org/10.1088/2053-1591/ac1f4c.
[36] Ma CP, Guan YC, Zhou W. Laser polishing of additive manufactured Ti alloys. Opt Laser Eng 2017;93:171–7. https://doi.org/10.1016/j.optlaseng.2017.02.005.
[37] Jaritngam P, Tangwarodomnukun V, Qi H, Dumkum C. Surface and subsurface characteristics of laser polished Ti6Al4V titanium alloy. Opt Laser Technol 2020; 126:106102. https://doi.org/10.1016/j.optlastec.2020.106102.
[38] Chen C, Tsai HL. Fundamental study of the bulge structure generated in laser polishing process. Opt Laser Eng 2018;107:54–61. https://doi.org/10.1016/j.optlaseng.2018.03.006.
[39] Kayahan E. A post-processing study on aluminum surface by fiber laser: removing face milling patterns. Opt Laser Technol 2018;101:440–5. https://doi.org/10.1016/j.optlastec.2017.11.042.
[40] Parameswari G, Jain VK, Ramkumar J, Nagdeve L. Experimental investigations into nanofinishing of Ti6Al4V flat disc using magnetorheological finishing process. Int J Adv Manuf Tech 2019;100:1055–65. https://doi.org/10.1007/s00170-017-1191-3.
[41] Zou YH, Xie HJ, Dong CW, Wu JZ. Study on complex micro surface finishing of alumina ceramic by the magnetic abrasive finishing process using alternating magnetic field. Int J Adv Manuf Tech 2018;97:2193–202. https://doi.org/10.1007/s00170-018-2064-0.
[42] Jain VK. Magnetic field assisted abrasive based micro-/nano-finishing. J Mater Process Tech 2009;209:6022–38. https://doi.org/10.1016/j.jmatprotec.2009.08.015.
[43] Barman A, Das M. Nano-finishing of bio-titanium alloy to generate different surface morphologies by changing magnetorheological polishing fluid compositions. Precis Eng 2018;51:145–52. https://doi.org/10.1016/j.precisioneng.2017.08.003.
[44] Barman A, Das M. Toolpath generation and finishing of bio-titanium alloy using novel polishing tool in MFAF process. Int J Adv Manuf Tech 2019;100:1123–35. https://doi.org/10.1007/s00170-017-1050-2.
[45] Fan ZH, Tian YB, Liu ZQ, Shi C, Zhao YG. Investigation of a novel finishing tool in magnetic field assisted finishing for titanium alloy Ti-6Al-4V. J Manuf Process 2019;43:74–82. https://doi.org/10.1016/j.jmapro.2019.05.007.
[46] Wang CJ, Cheung CF, Ho LT, Yung KL, Kong LB. A novel magnetic field-assisted mass polishing of freeform surfaces. J Mater Process Tech 2020;279:116552. https://doi.org/10.1016/j.jmatprotec.2019.116552.
[47] Loh YM, Gao R, Cheung CF, Chen YN, Li X, Li XG, Tsoi JKH, Wang CJ. A novel magnetic field assisted automatic batch polishing method for dental ceramic crowns. Ceram Int 2023;49:26540–7. https://doi.org/10.1016/j.ceramint.2023.05.188.
[48] Wang CJ, Loh YM, Cheung CF, Wang SX, Ho LT, Li Z. Shape-adaptive magnetic field-assisted batch polishing of three-dimensional surfaces. Precis Eng 2022;76: 261–83. https://doi.org/10.1016/j.precisioneng.2022.04.003.
[49] Wang CJ, Loh YM, Cheung CF, Wang SX, Chen KW, Ho LT, Cheng ER. Magnetic field-assisted batch superfinishing on thin-walled components. Int J Mech Sci 2022; 223:107279. https://doi.org/10.1016/j.ijmecsci.2022.107279.
[50] Liang XL, Liu ZQ, Liu WT, Wang B, Yao GH. Surface integrity analysis for high-pressure jet assisted machined Ti-6Al-4V considering cooling pressures and injection positions. J Manuf Process 2019;40:149–59. https://doi.org/10.1016/j.jmapro.2019.03.020.
[51] Krivková T, Tichy A, Tycova H, Kucera J. The influence of various adhesive systems and polishing methods on enamel surface roughness after debonding of orthodontic brackets: a three-dimensional in vitro evaluation. Materials 2023;16: 5107. https://doi.org/10.3390/ma16145107.
[52] Yamaguchi H, Shinmura T. Study of an internal magnetic abrasive finishing using a pole rotation system - discussion of the characteristic abrasive behavior. Precis Eng 2000;24:237–44. https://doi.org/10.1016/S0141-6359(00)00037-4.
[53] Ke XL, Wu W, Wang CJ, Yu YH, Zhong B, Wang ZZ, Wang TY, Fu JJ, Guo J. Material removal and surface integrity analysis of Ti6Al4V alloy after polishing by flexible tools with different rigidity. Materials 2022;15:1642. https://doi.org/10.3390/ma15051642.
[54] Lee JY, Jang GW, Park II, Heo YR, Son MK. The effects of surface grinding and polishing on the phase transformation and flexural strength of zirconia. J Adv Prosthodont 2019;11:1–6. https://doi.org/10.4047/jap.2019.11.1.1.
[55] Wang JH, Zhou Y, Qiao Z, Goel S, Wang JH, Wang X, Chen HY, Yuan JL, Lyu B. Surface polishing and modification of Ti-6Al-4V alloy by shear thickening polishing. Surf Coat Tech 2023;468:129771. https://doi.org/10.1016/j.surfcoat.2023.129771.
[56] Yu BJ, Gu Y, Lin JQ, Liu SL, Zhang S, Kang MS, Xi Y, Gao YH, Zhao HB, Ye QS. Surface polishing of CoCrMo alloy by magnetorheological polishing. Surf Coat Tech 2023;475:130162. https://doi.org/10.1016/j.surfcoat.2023.130162.
[57] Chen RF, Xu JM, Zhao FH, Wu YC, Zhang JJ. Preparation of microstructure laser ablation and multiple acid-etching composites on the surfaces of medical titanium alloy TC4 by laser ablation and multiple acid-etching, and study of frictional properties of the processed surfaces. Metals-Basel 2022;12:1148. https://doi.org/10.3390/met12071148.

[58] Wei Heping HY, Liu Zhaoyang. Experimental investigation on the surface integrity of titanium alloy TC4 in abrasive belt grinding. Adv Mater Res 2013;716:185–90. https://doi.org/10.4028/www.scientific.net/AMR.716.185.

[59] Li PF, Wang YH, Li LL, Gong YD, Zhou JZ, Lu JZ. Ablation oxidation and surface quality during laser polishing of TA15 aviation titanium alloy. J Mater Res Technol 2023;23:6101–14. https://doi.org/10.1016/j.jmrt.2023.02.209.

[60] Perry TL, Werschmoeller D, Li XC, Pfefferkorn FE, Duffie NA. The effect of laser pulse duration and feed rate on pulsed laser polishing of microfabricated nickel samples. J Manuf Sci E-T Asme 2009;131:310021–7. https://doi.org/10.1115/1.3106033.

[61] Liang CL, Liu WL, Li SS, Kong H, Zhang ZF, Song ZT. A nano-scale mirror-like surface of Ti-6Al-4V attained by chemical mechanical polishing. Chinese Phys B 2016;25:058301. https://doi.org/10.1088/1674-1056/25/5/058301.

[62] Yang X, Yang XZ, Kawai K, Arima K, Yamamura K. Highly efficient planarization of sliced 4H-SiC (0001) wafer by slurryless electrochemical mechanical polishing. Int J Mach Tool Manu 2019;144:103431. https://doi.org/10.1016/j.ijmachtools.2019.103431.

[63] Yan JW, Pan JS, Yan QS, Zhou R, Wu YS. Controllable electrochemical-magnetorheological finishing of single-crystal gallium nitride wafers. J Solid State Electr 2023;27:597–610. https://doi.org/10.1007/s10008-022-05322-8.